

# Ultrafast measurements under anisotropic strain reveal near equivalence of competing charge orders in TbTe<sub>3</sub>

Soyeun Kim,<sup>1,2</sup> Gal Orenstein,<sup>1,2</sup> Anisha G. Singh,<sup>2</sup> Ian R. Fisher,<sup>2</sup> David A. Reis,<sup>1,2</sup> and Mariano Trigo<sup>1,2</sup>

<sup>1</sup>Stanford PULSE Institute, SLAC National Accelerator Laboratory, Menlo Park, CA 94025, United States

<sup>2</sup>Stanford Institute for Materials and Energy Sciences,

SLAC National Accelerator Laboratory, Menlo Park, CA 94025, USA

(Dated: February 1, 2024)

We report ultrafast reflectivity measurements of the dynamics of the order parameter of the charge density wave (CDW) in TbTe<sub>3</sub> under anisotropic strain. We observe an increase in the frequency of the amplitude mode with increasing tensile strain along the  $a$ -axis (which drives the lattice into  $a > c$ , with  $a$  and  $c$  the lattice constants), and similar behavior for tensile strain along  $c$  ( $c > a$ ). This suggests that both strains stabilize the corresponding CDW order and further support the near equivalence of the CDW phases oriented in  $a$ - and  $c$ -axis, in spite of the orthorhombic space group. The results were analyzed within the time-dependent Ginzburg-Landau framework, which agrees well with the reflectivity dynamics. The strain dependence suggests that the orthogonal  $a$  and  $c$  CDWs are separately stabilized under the corresponding  $a > c$  and  $c > a$  strain, respectively. Our study presents an ultrafast approach to assess the stability of phases and order parameter dynamics in strained systems.

A central problem in condensed matter physics is understanding and controlling emergent phases in complex materials. Hydrostatic pressure and strain engineering, which can modify exchange couplings and inter-site hopping energies, are particularly fruitful approaches for inducing new phases [1–7]. Compared to hydrostatic pressure or epitaxial strain, uniaxial or highly anisotropic strain can more effectively lower the lattice symmetry and induce new states with different broken symmetries. This can have a qualitative impact on systems with competing phases, a prime example being nematic order in FeSe and its relation to superconductivity [8, 9].

The rare-earth tri-tellurides,  $R\text{Te}_3$  ( $R$  = rare earth ions), provide an attractive platform to realize uniaxial strain-controlled phases and control of competing orders. These materials exhibit two competing charge density wave (CDW) instabilities along two perpendicular crystallographic axes with almost identical lattice parameters ( $a = 4.3081(10)$  and  $c = 4.3136(10)$  for TbTe<sub>3</sub> at room temperature [10]). Chemical pressure [11, 12] as well as hydrostatic pressure [2, 3, 13] have been shown to tune the CDW instability and even enhance superconductivity at high pressure [14], suggesting that the equilibrium phase can be tuned with strain. Since the CDWs are hosted in the near-square, quasi-two-dimensional Te layers [11], anisotropic strain in the  $a$ - $c$  plane has the potential for tuning the near-degeneracy between the two perpendicular CDWs.

In this work, we present ultrafast reflectivity measurements of the dynamics of the CDW order parameter in TbTe<sub>3</sub> under anisotropic strain at room temperature. Unlike equilibrium measurements, ultrafast spectroscopy can provide crucial information on the single-particle and collective modes of the CDW [15–17]. By virtue of its nonequilibrium nature, pump-probe spectroscopy can unveil valuable information inaccessible by

other means. For example, nonlinear dynamics of the order parameter under high excitation reveal the anharmonic shape of the potential energy [18–21], and provides deeper insights into the broken symmetry phase.

Recent experiments give support to the near equivalence of the two CDWs in  $R\text{Te}_3$ . Ultrafast electron diffraction (UED) studies have shown an emergent CDW with wavevector in the  $a$  direction after photoexcitation quenches the equilibrium  $c$ -axis CDW [22]. Equilibrium x-ray diffraction measurements showed a similar rotation of the CDW wavevector by 90 degrees (from the  $c$ -axis to the  $a$ -axis) with tensile strain along the  $a$ -axis [23, 24]. These results suggest an intimate relationship between the  $a$ - and  $c$ -axes instabilities, a near equivalence between these two directions, and an emergent tetragonal symmetry proposed in ErTe<sub>3</sub> [23].

Our ultrafast reflectivity measurements on TbTe<sub>3</sub> show a stiffening of the CDW amplitude mode (AM) for a strong enough tensile strain along the  $a$ -axis, which is known to reorient the CDW wavevector by 90 degrees from the  $c$ - to the  $a$ -axis [23, 24]. This stiffening indicates that strain further stabilizes the order parameter of the rotated CDW for  $a > c$ . On the other hand, tensile strain along the  $c$ -axis ( $c > a$ ), also stiffens the original AM. These observations indicate a strong similarity between the potential energy surface of the two CDWs and further supports the proposed near equivalence between the  $c$  and  $a$  orders.

We analyze the reflectivity dynamics within the framework of the time-dependent Ginzburg-Landau model [16, 18, 19]. Our analysis of the coherent order parameter dynamics indicates that the system stiffens and develops a deeper free energy minimum for either  $a/c < 1$  or  $a/c > 1$ , which further stabilizes the  $c$  and  $a$  order, respectively. The near identical behavior for the two strain regimes is a signature of the near equivalence of the two

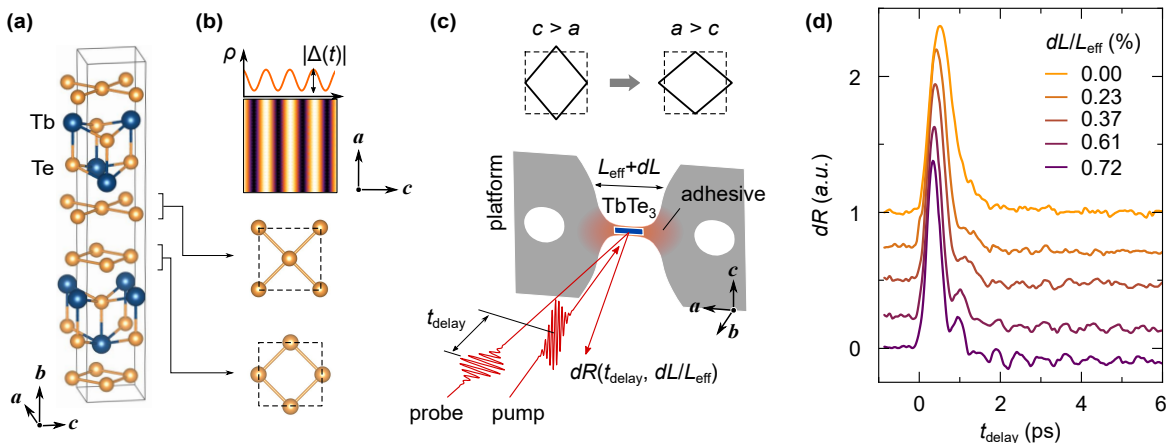


FIG. 1. (a) The crystal structure of  $\text{TbTe}_3$  in the  $Cmcm$  space group, featuring nearly tetragonal Te bilayers that separate TbTe blocks. (b) A schematic representation of the charge density ( $\rho$ ) amplitude ( $|\Delta|$ ) in real space. The charge-density-wave (CDW) phase forms along the  $c$ -axis at room temperature, with a cross-section along the  $c$ -axis displayed at the top of the image. (c) An illustration of the strain-dependent transient reflectivity setup. The sample is attached to the bowtie platform and experiences the anisotropic strain along the  $a$ -axis.  $L_{\text{eff}}$  denotes the effective distance, and  $dL$  the applied displacement. Two near-normal 800 nm pump and probe beams are incident onto the sample. (d) The transient time traces for various  $dL$  values, each displayed with an offset.

CDWs.

The crystal structure of the bulk  $\text{TbTe}_3$  belongs to the  $Cmcm$  space group (No. 63), and  $\text{TbTe}_3$  undergoes a CDW phase transition at  $T_{\text{CDW}} = 336$  K [11]. As in other series of the  $R\text{Te}_3$  family, the system is orthorhombic as depicted in Fig. 1(a). At room temperature, the  $c$  lattice constant is larger than  $a$  by 0.13 % and the CDW wavevector  $\mathbf{q}_{\text{CDW}}$  is oriented along the  $c$ -axis, as in Fig. 1(b). The difference between  $a$  and  $c$  reduces at higher temperatures and the CDW becomes unstable.

The small in-plane anisotropy is considered crucial for determining the direction of the CDW in  $R\text{Te}_3$ . Recent x-ray diffraction studies on the anisotropic-strain dependence on  $\text{ErTe}_3$  and  $\text{TbTe}_3$  have demonstrated the CDW can be reoriented by controlling the lattice constant ratio  $a/c$  [23, 24]. Because applying strain does not remove the glide plane, the  $C_4$  rotation symmetry remains absent, as in the pristine crystal. Nevertheless, x-ray diffraction measurements showed that the CDW wavevector rotates by  $90^\circ$  with increasing  $a/c$  [23]. Resistivity measurements under strain confirmed that the transition temperature increases as  $a/c$  deviates further from 1 for both  $a/c < 1$  and  $a/c > 1$  [23, 24], suggesting that strain stabilizes the respective  $c$  or  $a$  CDW.

To manipulate the CDW state in  $\text{TbTe}_3$ , an anisotropic strain field was applied along the  $a$ -axis using a CS-130 Razorbill strain cell device [25]. As depicted in Fig. 1, the bulk  $\text{TbTe}_3$  was attached to the neck of the bowtie-shaped platform, following the approach in the  $\text{ErTe}_3$  study [23]. The sample was cleaved to a thickness of 5-10  $\mu\text{m}$  and to expose a fresh surface and installed onto the strain cell device for the reflectivity measurements.

The effective length  $L_{\text{eff}}$  of the bowtie neck where the strain is active is 3.47  $\mu\text{m}$  [23, 26], and the displacement change  $dL$  in the strain cell device is obtained from the internal capacitor equipped inside the cell [25]. It is noteworthy that for most values of  $dL$  we used, the platform approaches or exceeds the plastic deformation limit of the titanium bowtie. This indicates the actual strain applied on the sample that affects the  $a/c$  may not have a linear relation with  $dL$ . Further details are provided in Ref. [23] and in the Supplementary Material [27].

The transient reflectivity time traces were obtained from an optical pump-probe setup using a Coherent RegA laser with 800 nm wavelength at a 250 kHz repetition rate. The probe (pump) beam had a  $1/e^2$  width of 40 (170)  $\mu\text{m}$  with a near-normal incident angle, which passed through a neutral density filter to change the fluence. The polarization of probe and pump beams were orthogonal to each other. The photon energy 1.55 eV is much higher than the CDW optical gap of  $\text{TbTe}_3$  at room temperature (220 meV) [12]. The pulse duration of the pump and probe beams was around 70 fs at the sample position, and the pump-probe delay was controlled with a mechanical delay stage.

Figure 1(d) presents the strain-dependent time traces of the transient reflectivity at room temperature. The scans were initiated from the maximum  $dL/L_{\text{eff}}$  and sequentially lowered (bottom to top traces) to minimize the extrinsic change in the reflectivity, such as crack formation.

The general features observed in the traces depicted in Fig. 1(d) align with findings from previous transient reflectivity studies on  $R\text{Te}_3$  [15, 18, 19, 28]. The shape of

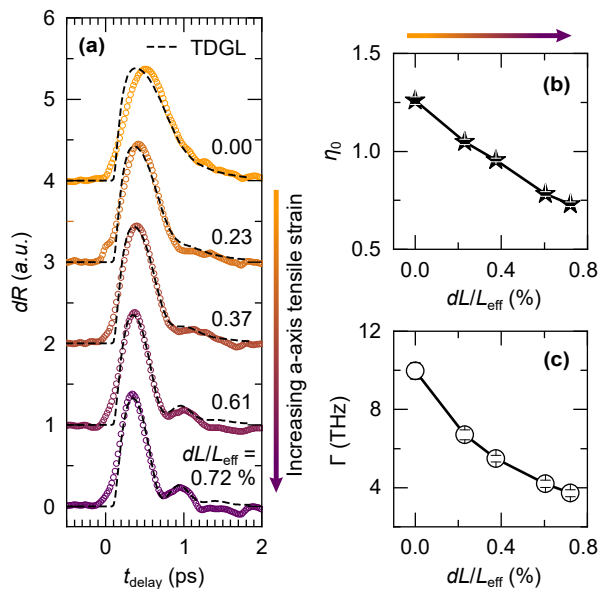


FIG. 2. (a) Transient reflectivity traces under tensile strain along the  $a$ -axis. Traces are offset vertically for clarity. The incident pump fluence was kept at  $9 \mu\text{J}/\text{cm}^2$  for all traces. The fit using the time-dependent Ginzburg-Landau (TDGL) model with  $\beta = 2.5$  THz and  $\Omega/2\pi = 2.2$  THz are overlaid with dashed lines. (b-c) Results of the fits (b)  $\eta_0$  and (c)  $\Gamma$ .

the initial peak relates to the initial order parameter dynamics, and the rise time of the peak was interpreted as the time needed to fully suppress the CDW order [28]. Phenomenological Ginzburg-Landau models based on quartic potentials successfully describe the trend in transient reflectivity at different temperatures and over a wide range of pump fluences, including at high fluence where nonlinearities in the lattice motion become important [18–20].

We now investigate how anisotropic strain affects the order parameter dynamics. When no strain is applied (top trace in Fig. 1(d);  $dL/L_{\text{eff}} = 0$  %), the time trace shows a smooth peak about 0.5 ps after the pump. A second hump starts to appear at 1.2 ps and becomes sharper with increasing  $dL/L_{\text{eff}}$  (lower traces in Fig. 1(d)). Additional oscillating features become discernible for time range of about 1.5 to 6 ps, which are prominent at  $dL/L_{\text{eff}} = 0.72\%$  (see Fig. S3 in the Supplemental Materials for details [27]).

The early dynamics of the reflectivity, *i.e.*, the initial peak and the second hump, are dominated by the CDW amplitude mode [19] and dynamic critical slowing down [28]. After 1.5 ps, the trace is dominated by coherent oscillation of 1.65 THz [27] from an optical phonon coupled to the AM [15]. In our analysis below, we focus on the behavior at  $t < 1$  ps, which reflect the order parameter dynamics in the dynamic critical slowing down regime.

The initial peak shows dramatic change with  $dL/L_{\text{eff}}$ ,

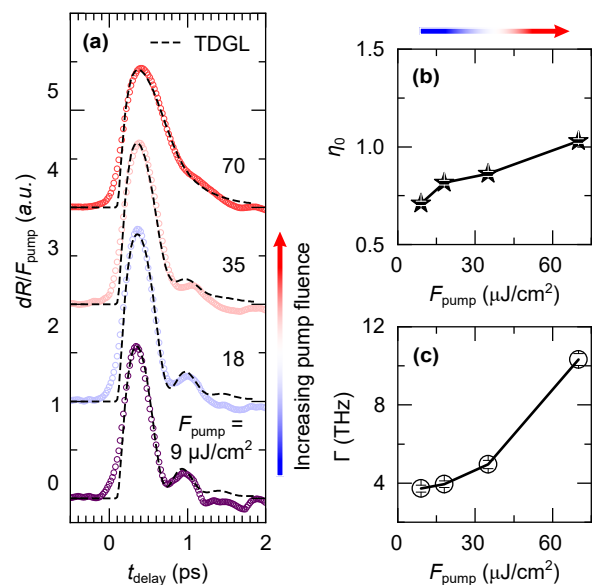


FIG. 3. (a) Fluence dependent time traces of transient reflectivity under applied  $a$ -axis tensile strain ( $dL/L_{\text{eff}} = 0.72$  %). Each trace is normalized by fluence and offset vertically. The fit using the TDGL with  $\beta = 2.5$  THz and  $\Omega/2\pi = 2.2$  THz are overlaid with dashed lines. (b-c) Results of the fits for (b)  $\eta_0$  and (c)  $\Gamma$ .

as shown in Fig. 2(a). With increasing tensile strain along the  $a$ -axis (increasing  $dL/L_{\text{eff}}$ ), the peak position shifts to earlier in time, the peak intensity first increases and then decreases, and the peak sharpens. For traces without vertical offsets, see Fig. S3 in the Supplemental Materials [27]. Importantly, the oscillations of the order parameter become more defined at higher  $dL/L_{\text{eff}}$  (see second cycle at  $t = 1$  ps in  $dL/L_{\text{eff}} = 0.72$  %). This occurs because of both a decrease in the damping and an increase in the frequency of the AM at higher strain.

The rise time of the peak  $\tau$  is related to the period of the AM, which diverges (the AM frequency vanishes) at the critical point in equilibrium. Thus, the decrease in  $\tau$  and decrease in the AM damping (better-defined AM oscillations) with increasing  $dL/L_{\text{eff}}$  observed here implies that the order parameter becomes more robust with increasing  $dL/L_{\text{eff}}$ , and that the system is pushed away from the critical point by further stabilizing the ordered phase. The initial peak dynamics showed a similar CDW stabilizing trend when the tensile strain was applied along the  $c$ -axis (see Fig. S5 in Supplemental Materials [27]).

To gain further insight into the strain-dependency in the transient reflectivity, we analyze the traces using the time-dependent Ginzburg-Landau (TDGL) model for second-order phase transitions, which has provided a good phenomenological description of the CDW order parameter dynamics in  $R\text{Te}_3$  [18–20, 28, 29]. Following Ref.

[19], the model is constructed by assuming the real dimensionless order parameter  $y$ , which is the amplitude of the CDW distortion at  $\mathbf{q}_{\text{CDW}}$ . With normalizing factor  $x_0$ , the effective potential can be represented with  $y$  as

$$V(y) = \frac{ax_0^2}{4}(2(\eta - 1)y^2 + y^4), \quad (1)$$

and the dynamics of  $y$  are governed by the equation of motion

$$\frac{1}{a}\ddot{y} + [\eta(t) - 1]y + y^3 + \frac{2\Gamma}{a}\dot{y} = 0. \quad (2)$$

Here  $a = 95.54 \text{ THz}^2$  is related to the AM angular frequency  $\Omega$  by  $a = \Omega^2/2$ ,  $\Gamma$  is a phenomenological damping, and  $\eta$  is a parameter that controls the stability of the CDW [19]. In equilibrium,  $\eta = T/T_{\text{CDW}}$ , *i.e.*,  $\eta = 0$  indicate the CDW ground state, and  $\eta > 1$  represents the free energy of the high-symmetry phase [18, 19]. To introduce the transient change triggered by the optical pump, we take  $\eta(t) = \eta_0 e^{-\beta t} \Theta(t)$ , where  $\Theta(t)$  is a step function and  $\beta$  is the decay rate of the electronic excitation [19, 27].

We now relate the order parameter  $y(t)$  to the reflectivity. The expansion of the reflectivity in terms of the order parameter is quadratic in  $y$  [1, 19] which by symmetry must be insensitive to the sign of  $y$ . Thus we fit the time traces using the function  $A(1 - y^2(t))$ ,  $A$  being an amplitude (See Fig. S1 in Supplemental Materials). We fixed  $\Omega/2\pi$  to the AM frequency 2.2 THz in unstrained TbTe<sub>3</sub> at low temperature [15]. To minimize the number of the parameters we fit only  $\eta_0$  and  $\Gamma$  and kept the relative zero time delay,  $A$ , and  $\beta$  fixed.

Figure 2 presents the fit results of the TDGL model to reflectivity traces for the AM dynamics at  $t < 2$  ps. Overall, the fit curves in panel (a) capture the main features in each trace described earlier, including the trend with increasing strain. The fitted  $\eta_0$  values in (b) show a gradual decrease with increasing  $dL/L_{\text{eff}}$ . The value of  $\Gamma$  (damping rate) also decreases with increasing strain, indicating that the order parameter is more harmonic (less damped) and its dynamics last about 2.5 times longer in the 0.72 % trace than for the 0 %. The results of the fits in Figs. 2(b,c) clearly show that the  $a$ -axis tensile strain decreases  $\eta_0$  and  $\Gamma$ . This signifies that the strain pushes the potential energy into deeper double-well form (decreasing  $\eta$ ) as shown schematically in Fig. 4(a), hence stabilizing the CDW, which for  $a > c$  is rotated with respect to the unstrained CDW [23].

At higher pump fluence ( $F_{\text{pump}}$ ) an increase in  $\eta$  can destabilize the CDW order [27–29]. In Fig. 3, we verified the fluence dependence of the strain-stabilized CDW at  $dL/L_{\text{eff}} = 0.72$  %. The shape change in the initial peak with increasing  $F_{\text{pump}}$  is analogous to the trend with decreasing  $dL/L_{\text{eff}}$  in Fig. 2. The gradual broadening (increasing  $\tau$ ) and faster damping of the oscillation at high  $F_{\text{pump}}$  again indicate that  $\eta_0$  and  $\Gamma$  increase with  $F_{\text{pump}}$ .

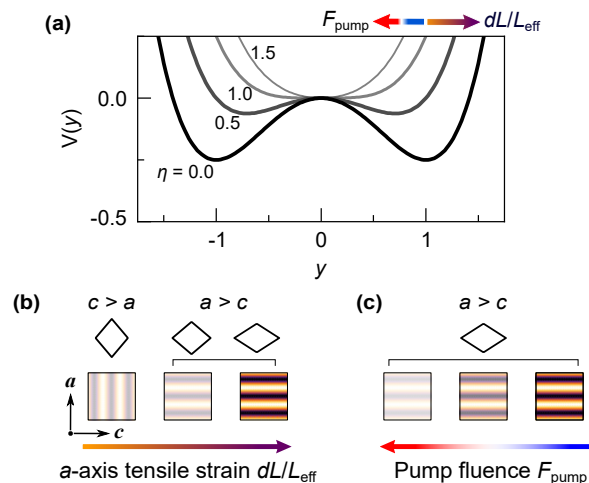


FIG. 4. (a) The Ginzburg-Landau potential  $V(y)$  shape for the representative  $\eta$  values. (b-c) Schematic diagrams of the CDW affected by increasing (b) the  $a$ -axis tensile strain and (c) pump fluence under strain. The arrows in (a) indicate the change in the potential driven by  $dL/L_{\text{eff}}$  or  $F_{\text{pump}}$ .

The values extracted from the TDGL fits are shown in Figs. 3(b,c) and are comparable with fluence dependence in prior measurements on SmTe<sub>3</sub> [19].

Figure 4 summarizes the behavior of the Ginzburg-Landau potential with the  $a$ -axis tensile strain and pump fluence, extracted from Figs. 2 and 3, respectively. As mentioned earlier, prior strain studies on ErTe<sub>3</sub> and TbTe<sub>3</sub> demonstrated that the CDW wavevector is rotated from the  $c$ - to the  $a$ -axis when  $a > c$  [23, 24]. As the in-plane anisotropy grows, the reoriented CDW is further stabilized, making the potential well deeper and hardening the AM frequency, as evidenced by the observed decrease in  $\tau$  and corresponding decrease in the fitted  $\eta_0$  (Fig. 2 (b)) with increasing  $dL/L_{\text{eff}}$ .

The fact that both CDWs can be modeled with similar parameters within TDGL by using the same AM frequency ( $\Omega/2\pi = 2.2$  THz) suggests that the original (unstrained) and reoriented CDW are virtually indistinguishable and that they originate from the same free energy instability and further supports the interpretation that the original (with wavevector along  $c$ ) and reoriented (with wavevector along  $a$ ) CDW phases are nearly equivalent [23].

To conclude, we used ultrafast optical spectroscopy to probe the dynamics of the order parameter in TbTe<sub>3</sub> under anisotropic strain. The response when  $a/c < 1$  and  $a/c > 1$  is nearly identical and both CDWs can be modeled with the same Ginzburg-Landau potential despite the intrinsically orthorhombic nature of the underlying lattice, which further supports the near equivalence of the two CDWs. These results demonstrate a versa-

tile tool combining ultrafast spectroscopy with uniaxial strain tuning device to probe the potential energy surfaces and low energy excitations of competing orders in quantum materials.

S.K., V.K., A.G.S., I.R.F., D.A.R., and M.T. were supported by the US Department of Energy, Office of Science, Office of Basic Energy Sciences through the Division of Materials Sciences and Engineering under Contract No. DE-AC02-76SF00515. G.O. acknowledges support from the Koret Foundation.

- 
- [1] V. L. Ginzburg, Soviet Physics Uspekhi **5**, 649–660 (1963).
- [2] A. Sacchetti, E. Arcangeletti, A. Perucchi, L. Baldassarre, P. Postorino, S. Lupi, N. Ru, I. R. Fisher, and L. Degiorgi, Physical Review Letters **98**, 026401 (2007).
- [3] D. A. Zocco, J. J. Hamlin, K. Grube, J.-H. Chu, H.-H. Kuo, I. R. Fisher, and M. B. Maple, Physical Review B **91**, 205114 (2015).
- [4] D. G. Schlom, L.-Q. Chen, C.-B. Eom, K. M. Rabe, S. K. Streiffer, and J.-M. Triscone, Annual Review of Materials Research **37**, 589–626 (2007).
- [5] D. G. Schlom, L.-Q. Chen, C. J. Fennie, V. Gopalan, D. A. Muller, X. Pan, R. Ramesh, and R. Uecker, MRS Bulletin **39**, 118–130 (2014).
- [6] R. Xu, J. Huang, E. S. Barnard, S. S. Hong, P. Singh, E. K. Wong, T. Jansen, V. Harbola, J. Xiao, B. Y. Wang, S. Crossley, D. Lu, S. Liu, and H. Y. Hwang, Nature Communications **11** (2020).
- [7] C. Ji, B. Li, W. Liu, J. S. Smith, A. Majumdar, W. Luo, R. Ahuja, J. Shu, J. Wang, S. Sinogeikin, Y. Meng, V. B. Prakapenka, E. Greenberg, R. Xu, X. Huang, W. Yang, G. Shen, W. L. Mao, and H.-K. Mao, Nature **573**, 558–562 (2019).
- [8] M. Ghini, M. Bristow, J. C. A. Prentice, S. Sutherland, S. Sanna, A. A. Haghighirad, and A. I. Coldea, Physical Review B **103**, 205139 (2021).
- [9] S. Hosoi, K. Matsuura, K. Ishida, H. Wang, Y. Mizukami, T. Watashige, S. Kasahara, Y. Matsuda, and T. Shibauchi, Proceedings of the National Academy of Sciences **113**, 8139–8143 (2016).
- [10] N. Ru, *Charge density wave formation in rare-earth tritellurides*, Ph.D. thesis, Stanford University (2008).
- [11] N. Ru, C. L. Condrón, G. Y. Margulis, K. Y. Shin, J. Laverock, S. B. Dugdale, M. F. Toney, and I. R. Fisher, Physical Review B **77**, 035114 (2008).
- [12] B. F. Hu, B. Cheng, R. H. Yuan, T. Dong, and N. L. Wang, Physical Review B **90**, 085105 (2014).
- [13] J. Kopaczek, H. Li, K. Yumigeta, R. Sailus, M. Y. Sayyad, S. T. R. Moosavy, R. Kudrawiec, and S. Tongay, Journal of Materials Chemistry C **10**, 11995–12000 (2022).
- [14] J. J. Hamlin, D. A. Zocco, T. A. Sayles, M. B. Maple, J. H. Chu, and I. R. Fisher, Physical Review Letters **102** (2009).
- [15] R. V. Yusupov, T. Mertelj, J.-H. Chu, I. R. Fisher, and D. Mihailovic, Physical Review Letters **101**, 246402 (2008).
- [16] H. Schaefer, V. V. Kabanov, and J. Demsar, Physical Review B **89**, 045106 (2014).
- [17] A. S. Disa, T. F. Nova, and A. Cavalleri, Nature Physics **17**, 1087 (2021).
- [18] R. Yusupov, T. Mertelj, V. V. Kabanov, S. Brazovskii, P. Kusar, J.-H. Chu, I. R. Fisher, and D. Mihailovic, Nature Physics **6**, 681 (2010).
- [19] M. Trigo, P. Giraldo-Gallo, M. E. Kozina, T. Henighan, M. P. Jiang, H. Liu, J. N. Clark, M. Chollet, J. M. Glowina, D. Zhu, T. Katayama, D. Leuenberger, P. S. Kirchmann, I. R. Fisher, Z. X. Shen, and D. A. Reis, Physical Review B **99**, 104111 (2019).
- [20] M. Trigo, P. Giraldo-Gallo, J. N. Clark, M. E. Kozina, T. Henighan, M. P. Jiang, M. Chollet, I. R. Fisher, J. M. Glowina, T. Katayama, P. S. Kirchmann, D. Leuenberger, H. Liu, D. A. Reis, Z. X. Shen, and D. Zhu, Physical Review B **103**, 054109 (2021).
- [21] G. Orenstein, R. A. Duncan, G. A. d. l. P. Munoz, Y. Huang, V. Krapivin, Q. L. Nguyen, S. Teitelbaum, A. G. Singh, R. Mankowsky, H. Lemke, M. Sander, Y. Deng, C. Arrell, I. R. Fisher, D. A. Reis, and M. Trigo, arXiv , 2304.00168 (2023).
- [22] A. Kogar, A. Zong, P. E. Dolgirev, X. Shen, J. Straquadine, Y.-Q. Bie, X. Wang, T. Rohwer, I.-C. Tung, Y. Yang, R. Li, J. Yang, S. Weathersby, S. Park, M. E. Kozina, E. J. Sie, H. Wen, P. Jarillo-Herrero, I. R. Fisher, X. Wang, and N. Gedik, Nature Physics **16**, 159–163 (2019).
- [23] A. G. Singh, M. D. Bachmann, J. J. Sanchez, A. Pandey, A. Kapitunik, J. W. Kim, P. J. Ryan, S. A. Kivelson, and I. R. Fisher, arXiv , 2306.14755 (2023).
- [24] A. Gallo-Frantz, A. Sinchenko, D. Ghoneim, L. Ortega, P. Godard, P.-O. Renault, P. Grigoriev, A. Hadj-Azzem, P. Monceau, D. Thiaudière, E. Bellec, V. Jacques, and D. L. Bolloc’h, arXiv , 2306.15712 (2023).
- [25] Cryostrain cell. Data sheet: CS130, Razorbill Instruments, 2023.
- [26] J. Park, J. M. Bartlett, H. M. L. Noad, A. L. Stern, M. E. Barber, M. König, S. Hosoi, T. Shibauchi, A. P. Mackenzie, A. Steppke, and C. W. Hicks, Review of Scientific Instruments **91**, 083902 (2020).
- [27] See Supplemental Material.
- [28] A. Zong, P. E. Dolgirev, A. Kogar, E. Ergeçen, M. B. Yilmaz, Y.-Q. Bie, T. Rohwer, I.-C. Tung, J. Straquadine, X. Wang, Y. Yang, X. Shen, R. Li, J. Yang, S. Park, M. C. Hoffmann, B. K. Ofori-Okai, M. E. Kozina, H. Wen, X. Wang, I. R. Fisher, P. Jarillo-Herrero, and N. Gedik, Physical Review Letters **123**, 097601 (2019).
- [29] J. Maklar, Y. W. Windsor, C. W. Nicholson, M. Puppin, P. Walmsley, V. Esposito, M. Porer, J. Rittmann, D. Leuenberger, M. Kubli, M. Savoini, E. Abreu, S. L. Johnson, P. Beaud, G. Ingold, U. Staub, I. R. Fisher, R. Ernstorfer, M. Wolf, and L. Rettig, Nature Communications **12**, 2499 (2021).